Molecular Catalysis 474 (2019) 110404

Contents lists available at ScienceDirect

Molecular Catalysis

journal homepage: www.elsevier.com/locate/mcat

Selective aerobic oxidation of glycerol over zirconium phosphate-supported vanadium catalyst

Difan Li[a], Honghui Gong[a], Lina Lin[b], Wenbao Ma[a], Qingqing Zhou[a], Kang Kong[a], Rong Huang[b,*], Zhenshan Hou[a,*]

[a] Key Laboratory for Advanced Materials, Research Institute of Industrial Catalysis, School of Chemistry and Molecular Engineering, East China University of Science and Technology, Shanghai, 200237, China
[b] Key Laboratory of Polar Materials and Devices, Ministry of Education, East China Normal University, Shanghai, 200062, China

ARTICLE INFO

Keywords:
Zirconium phosphate
Vanadium
Mechanochemical synthesis
Glycerol oxidation
Formic acid

ABSTRACT

The zirconium phosphate (ZrP)-supported vanadium catalysts have been prepared by the mechanochemical synthesis, and were characterized in detail using various techniques including XRD, SEM, HRTEM, EDX, NH_3-TPD, H_2-TPR, pyridine-absorbed FT-IR and solid ^{31}P NMR spectra. XRD, SEM and HRTEM images revealed the vanadium species were highly dispersed on ZrP support. Solid ^{31}P NMR technique indicated that there was a strong interaction between vanadium species and ZrP. The calcination temperature affected significantly the distribution for oxidation states of vanadium, and the presence of vanadium (V) species were more favorable to the glycerol oxidation reaction. The resulting catalysts exhibited high catalytic activity for glycerol oxidation and the selectivity to formic acid in glycerol oxidation by using molecular oxygen as the terminal oxidant under the aqueous phase and base-free conditions. Both acid sites and oxidizing sites played a synergistic role in producing the compounds in this work. The reaction can proceed smoothly with high glycerol conversion up to 80–90% and the selectivity towards formic acid to 62%, respectively. After reaction, the catalyst can be facilely recovered and reused with stable activity. On the basis of the above results, the reaction mechanism was proposed accordingly. This study provides a prominent catalytic process for the large scale production of formic acid from biorenewable glycerol.

1. Introduction

With the progressively depleting of fossil fuel, such as the traditional petroleum, coal and natural gas resources, a large number of problems are brought forward [1]. The main disadvantage of fossil resource is nonrenewable, implying significant negative side effects are related to the sustainable development of the global economy and society, as well as exacerbating environmental pollution. In this respect, it is important to search alternative resources and develop new processes for the production of fine chemicals and fuels [2]. In recent years, one of the main renewable resources is biodiesel. Its main advantages lie in significant potential as a renewable energy source, biodegradability and less emission of air pollutants, which can be converted to more valuable compounds [3]. During the production process of biodiesel, an abundant and inexpensive glycerol is produced as a by-product by transesterification of fats and oils (triglycerides) with methanol, resulting in a high surplus flooding the market over the last decades (10% of the plant product) [4]. Therefore, the growing production of biodiesel is accompanied by increasing interest in the development of potential valorization strategies of glycerol [5,6].

Great efforts have been devoted on the catalytic conversion of glycerol into platform molecules and subsequently high value added chemicals by selective catalytic transformation owing to the fact that it is regarded as a highly functionalized molecule with three hydroxyl groups [7]. On one hand, because of its good water solubility and hygroscopicity, it can be widely used as a humectant in the food, medicine, cosmetics and tobacco industries. On the other hand, in order to substantially increase the demand and the price of crude glycerol and, hence, make the biodiesel production more economically feasible, it is necessary to investigate the transformation of glycerol into different derivatives and intermediates by new technologies and catalytic routes, such as hydrogenation, hydrolysis, oxidation, chlorination, etherification, esterification, transesterification and reforming [8]. Among those catalytic conversion processes, the selective oxidation of glycerol in liquid phase has been widely studied during the last decades with various catalytic systems involving precious metals (Au, Pt, Pd, Ag)

* Corresponding authors.
E-mail addresses: rhuang@ee.ecnu.edu.cn (R. Huang), houzhenshan@ecust.edu.cn (Z. Hou).

https://doi.org/10.1016/j.mcat.2019.110404
Received 17 November 2018; Received in revised form 14 April 2019; Accepted 13 May 2019

[9–13]. However, the use of noble metals presents economic challenges, owing to high costs, scarce resources, and these metal particles are easily agglomerated during the reaction and limit availability of large-scale application and production. In addition, the transition metals (Cu, Ni, Co, Fe) as catalysts are also explored [14–18], although the cost of this type of catalyst is not high, the catalytic activity is normally poor. These catalysts cannot be applied to practical production without further complicated modification. Besides, many catalytic systems involve the basic reaction medium. Due to its basicity, it produces a lot of organic acid salts and thus the mixtures after reaction need further neutralization and acidification so as to obtain the target products. Therefore, the exploration of new materials based on non-noble metal and base-free highly active systems become the focus of the catalysis field.

Formic acid (FA) is one important source of C1 raw materials in high demand for the chemical, leather, textile, pharmaceutical, agricultural industries. Particularly, FA is explored as a promising medium/carrier for hydrogen storage and an energy-efficient alternative for the sustainable hydrogen production based on reversible $FA-CO_2$ interconversion [19]. A diverse range of highly attractive products and building blocks can be derived from FA as well [20]. FA salts are also widely used for environmentally friendly runway de-icing and fuel in fuel cells [21]. Therefore, FA as a versatile renewable reagent for green and sustainable chemical synthesis has attracted substantial research interest in recent years. Industrial production technologies of FA gains mainly from fossil resources, which have an unfavorable impact on the environment [22]. Up to now, FA production from biomass has been demonstrated to be a promising process [23]. Developing alternative routes to produce FA directly from glycerol is desirable from both economic and ecological perspectives.

The various vanadium-based catalysts have been reported to catalyze the selective oxidation of alkanes, alkenes, arenes, alcohols, aldehydes, ketones, and sulfur species, as well as oxidative C − C or C − O bond cleavage, C − C bond formation, deoxydehydration, hydrogenation, dehydrogenation and polymerization [24]. Especially, the vanadium-based catalysts were highly active for the oxidations of biomass-derived carbohydrates [22,25–28] and saccharides [29,30]. Tremendous efforts have also been devoted to the selective oxidation of glycerol to FA with different oxidizing agents. In our previous report, the silica-encapsulated heteropolyacid ($H_4PMo_{11}VO_{40}$) can convert glycerol to FA selectively, but the process needs the aid of extra additives and also an excess of H_2O_2 as oxidant [31]. The vanadium-substituted phosphomolybdic acids could exhibit exceptionally high conversion efficiency in highly concentrated aqueous solutions with molecular oxygen as oxidant, but the isolation of water-soluble catalyst is difficult after reaction [32].

Zirconium phosphate (ZrP) as a family of transition metal phosphate materials, increasingly attracts research interest due to its outstanding physical and chemical properties, including an extremely high ion-exchange capability and excellent thermal stability. These superior properties, along with simple preparation and easy functionalization, making ZrP-based materials as promising candidates for a wide range of applications [33,34]. In this work, novel vanadium-based ZrPs are prepared without using any solvents by mechanochemical transformation. The ZrP can be found to act as an efficient support to immobilize vanadium source, wherein the surface P(OH) groups provide strong interaction toward vanadium species. Owing to such strong interaction, the obtained ZrP-supported vanadium catalysts show high activity and good reusability for the selective oxidation of glycerol to FA using molecular oxygen as the oxidant. Systematic activity tests and catalyst characterizations have been applied to identify the roles of ZrP and vanadium sites in FA formation in detail. Finally, the relationship of structure with catalytic activity is presented herein and possible reaction mechanism is proposed as well.

2. Experimental

2.1. Materials

All chemicals and solvents were commercially available and used as received without further purification. Zirconium oxychloride ($ZrOCl_2{\cdot}8H_2O$, 98 wt.%), hydroxyacetone (HA, 95 wt.%) and dihydroxyacetone (DHA, 99 wt.%) were provided by Macklin. Vanadium (IV) oxide sulfate ($VOSO_4$, AR) was acquired from Meryer. Vanadyl acetylacetonate ($VO(acac)_2$), ammonium vanadate (NH_4VO_3) and sodium metavanadate ($NaVO_3$) were all analytical reagent grade and purchased from Aladdin. Ammonium dihydrogen phosphate ($NH_4H_2PO_4$) and glycerol, were also analytical reagent grade and supplied by Sinopharm. Formic acid (FA, 98 wt.%), ethylene glycol (EG, 98 wt.%), acetic acid (AA, AR) and concentrated sulphuric acid (H_2SO_4, 98 wt.%) were all obtained from Lingfeng. High purity O_2 (99.9%). was supplied by Shangnong Gas Factory.

2.2. Catalyst preparation

2.2.1. Preparation of amorphous ZrP

The amorphous ZrP was prepared by a precipitation method according to the previous procedure [35]. Briefly, an aqueous solution of $NH_4H_2PO_4$ (1.0 mol L^{-1}, 64 mL) was added dropwise to an aqueous solution of $ZrOCl_2{\cdot}8H_2O$ (1.0 mol L^{-1}, 32 mL) at a molar ratio of P/Zr = 2. The mixture was stirred overnight at room temperature, then filtered, and washed with copious deionized water until the pH of the filtrate reached to neutral and free of Cl^-, which was detected by aqueous $AgNO_3$ solution. The resulting material was dried at 100 °C for 12 h, followed by calcination at 400 °C for 4 h in a muffle furnace and the solid powder was denoted as ZrP.

2.2.2. Preparation of catalysts

The ZrP-supported vanadium catalysts can be achieved by mechanochemical synthesis. As a typical example, 0.5 g ZrP and a certain amount of $VOSO_4$ were mixed in agate mortar, and then continuously grinded for 30 min. The resulting material was calcinated at 550 °C for 3 h in a muffle furnace, unless indicated otherwise. The obtained sample was named as *x*V/ZrP-m, *x* stands for the loading contents of vanadium on ZrP support. According to a similar method, NH_4VO_3, $NaVO_3$ and $VO(acac)_2$ as vanadium precursors afforded the corresponding catalysts 2 V_1/ZrP-m, 2 V_2/ZrP-m, 2 V_3/ZrP-m, respectively. No solvents were employed in the course of mechanochemical synthesis. For the sake of comparison, the ZrP-supported vanadium catalysts with the same contents were prepared by the incipient wetness method, and the resulting material was designated as 2 V/ZrP-i arisen from $VOSO_4$ as vanadium precursors.

2.3. Characterization

Powder X-ray diffraction (XRD) patterns were collected on a SmartLab diffractometer from Rigaku equipped with a 9 kW rotating anode Cu source at 45 kV and 100 mA (5–80°, 0.2° s^{-1}). Scanning electron microscope (SEM) accompanied by energy dispersive X-ray spectrometry (EDX; accelerated voltage: 20 kV) was used to study the morphology and the elements distribution (JEOL JSM-6360LV, Japan). High resolution transmission electron microscopy (HRTEM) was performed in a JEOL JEM 2010 transmission electron microscope operating at 200 kV with a nominal resolution of 0.25 nm. The samples for HRTEM were prepared by dropping the aqueous solutions containing the NPs onto the carbon-coated Cu grids. Nitrogen (N_2) adsorption isotherms and pore size distribution curves were measured at −196 °C on a BELSORP-MINI analyzer. The samples were degassed at 200 °C for 1 h to a vacuum of 10^{-3} Torr before analysis, The BET surface area and pore size distribution of the samples were calculated using the BET (Brunauer–Emmett–Teller) equation and the BJH

(Barrett–Joyner–Halenda) model, respectively. A Perkin Elmer Pyris Diamond was used for the TGA measurements. The samples were heated from RT to 800 °C (heating rate: 10 °C min^{-1}) under the flow of anhydrous air (flow rate: 20 mL min^{-1}). NH_3-Temperature programmed desorption (TPD) results were recorded using a BELCAT-B temperature programming unit equipped with a thermal conductivity detector (TCD). The forming CO_2 during the reaction was detected by gas chromatography (GC) with TCD. As a typical run, 0.1 g of catalyst was placed in a U-shaped quartz cell and preconditioned at 200 °C in He for 2 h, followed by cooling down to 40 °C in He flow. Then, the catalyst was saturated with ammonia (5% NH_3 balanced with He) at 40 °C for 45 min. Afterwards, the sample was exposed to He for removing of the physically adsorbed ammonia on the surface of the sample. Subsequently, the TPD profile was recorded upon heating the sample at a rate of 10 °C min^{-1} up to 800 °C. H_2-Temperature programmed reduction (TPR) was carried out using the glass flow system. TPR runs were performed in flowing 10% H_2/Ar (30 cm^3 min^{-1}), ramping the temperature at 10 °C min^{-1} and using a Gow-Mac TCD. Solid ^{13}C NMR spectra were recorded on a Bruker AVANCE-III spectrometer in a magnetic field strength of 9.4 T corresponding to the Larmor frequency of 500 MHz for ^{13}C nuclei with a CP/MAS unit at room temperature (spinning rate: 5 kHz; contact time: 2 ms; pulse width: 2 ms; spectral width: 42.6 kHz; acquisition time: 48.1 ms; 700 scans for each spectrum). The ^{13}C chemical shifts were referred by using tetramethylsilane as internal standard. Solid ^{31}P MAS NMR spectra were obtained with a VNMRS400WB spectrometer (162 MHz for ^{31}P nuclei) equipped with a standard 4 mm MAS NMR probe head. The ^{31}P chemical shifts were referred to $NH_4H_2PO_4$. The surface chemical composition was determined by X-ray photoelectron spectroscopy (XPS) on ESCALAB 250Xi equipped with Al Kα radiation (1486.6 eV). Metal contents were detected by an Agilent ICP-725 inductively coupling plasma atomic emission spectrometer (ICP-AES). The sample was put in a plastic beaker mixed with a certain amount of aqua regia and HF at 120 °C for 4 h to dissolve the sample easily, followed by diluted with deionized water. The FT-IR spectra of the pyridine-adsorbed on catalyst was obtained in the transmission mode using a Nicolet Model 710 spectrometer. First, the catalyst was ground into the powder and pressed into a very thin self-supporting wafer. The disc was mounted in a quartz IR cell equipped with a CaF_2 window. Then the catalyst was pressed into a self-supporting disk and placed in an IR cell attached to a closed glass circulation system. The catalyst disk was dehydrated by heating at 400 °C under vacuum in order to remove physisorbed moisture. The IR spectrum background was recorded at room temperature when the cell cooled down. Pyridine vapor was then introduced into the cell at room temperature until equilibrium was reached. Subsequent evacuations were performed at room temperature for 60 min followed by spectral acquisitions at room temperature using the background recorded before. The quantification of acid sites was performed using the same expressions (1) and (2) as those in the research article of Angela S. Rocha:

$$C_B = k_B A_{1540} = \frac{\pi}{IMEC_B}\left(\frac{r^2}{\omega}\right)A_{1540} \quad (1)$$

$$C_L = k_L A_{1450} = \frac{\pi}{IMEC_L}\left(\frac{r^2}{\omega}\right)A_{1450} \quad (2)$$

C_L and C_B are the concentrations of Lewis acid and Brönsted acid sites in μmol g^{-1}; A_{1450} and A_{1540} are the integrated areas of bands at 1450 and 1540 cm^{-1} in the original data of FTIR spectra, as shown in the section of Results and discussion. K_L and K_B are molar extinction constants for Lewis and Brönsted acid sites; $IMEC_L$ and $IMEC_B$ are integration molar extinction coefficients, 2.22 and 1.67 cm μmol $^{-1}$ for Lewis and Brönsted acids, respectively; r is the wafer radius in cm and ω is the wafer weight in g of the self-supporting catalyst disk.

2.4. Catalytic reaction

Glycerol oxidation was performed in a high-pressure batch autoclave of stainless steel with a 25 mL polytetrafluoroethylene inlet. The autoclave was equipped with gas supply system and a magnetic stirrer. Typically, a certain amount of catalyst was suspended in 5 mL aqueous glycerol (10 wt.%) and the autoclave was purged with oxygen for three times. Then it was sealed with the required oxygen pressure and heated to the set temperature in 30 min. The zero time was taken when the medium in the reactor was heated to the desired temperature. After the reaction was finished, the reactor was quenched in an ice-water bath to stop the reaction and the reaction mixture was diluted with deionized water then filtered with a 0.22 mm membrane filter before analysis. The liquid samples were analyzed by high performance liquid chromatography (HPLC) using equipped with a refractive index detector in series with Bio-Rad Aminex HPX-87H column together with a guard cartridge was employed for product separation. The column oven temperature was 50 °C, the mobile phase was diluted with a concentration of 5 mM H_2SO_4 aqueous solution and 0.5 mL min^{-1} flow rate, 20 μL of each sample was injected and peaks were detected with refractive index detector. The gas phase from the high-pressure batch autoclave was collected and analyzed quantitatively with TCD. All values determined for selectivity and carbon mass balance were provided by HPLC analysis. The conversion of glycerol and yield towards products were calculated as follows:

$$\text{Conversion (\%)} = \frac{\text{amount of glycerol converted (mole)}}{\text{total amount of glycerol (mole)}} \times 100\%$$

$$\text{Selectivity (\%)} = \frac{\text{amount of a product (mole)}}{\text{amount of glycerol converted (mole)}} \times \frac{\text{number of carbon atoms in the product}}{3} \times 100\%$$

$$\text{Carbon mass balance (\%)} = \frac{\text{carbon atoms found in the products (mole)}}{\text{carbon atoms of glycerol converted (mole)}} \times 100\%$$

3. Results and discussion

3.1. Catalyst characterization

The phase structures of the pristine $VOSO_4$, ZrP-supported vanadium catalysts are determined by the XRD patterns. As illustrated in

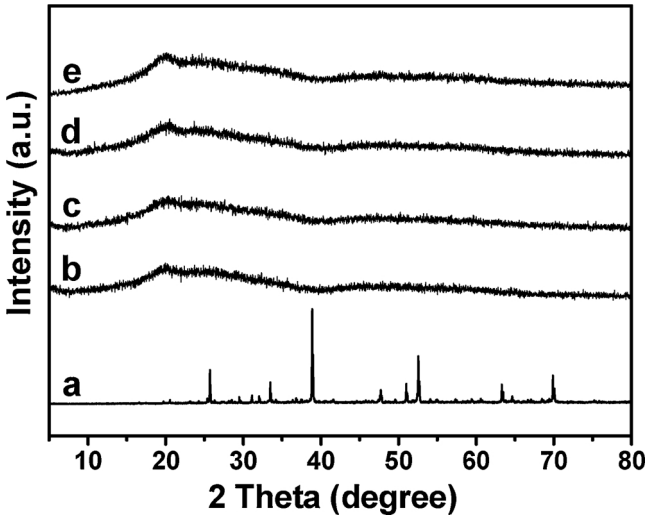

Fig. 1. XRD patterns of (a) $VOSO_4$ (b) ZrP, (c) 2 V/ZrP-m, (d) 2 V/ZrP-i and (e) the spent 2 V/ZrP-m.

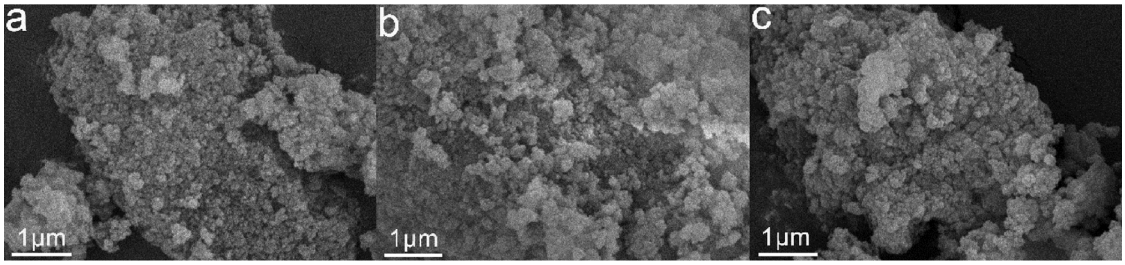

Fig. 2. SEM images of (a) ZrP, (b) 2 V/ZrP-m and (c) the spent 2 V/ZrP-m catalyst.

Fig. 1a, neat $VOSO_4$ displays a set of well resolved sharp diffraction peaks for the typical crystal structure of $VOSO_4$ (JCPDS No. 019–1411) [36]. The catalysts including ZrP, 2 V/ZrP-m and 2 V/ZrP-i mainly show two broad peaks in the ranges of 10–40° and 40–70°, indicating that they are all amorphous nature and the introduction of vanadium by either mechanochemical synthesis or incipient wetness method actually has no effect on the crystal structure of ZrP (Fig. 1b–d). In addition, either increasing vanadium contents (from 1% to 10%), or using the different vanadium precursors have no effect on the amorphous phase of ZrP (Figure S1 and S2). Notably, the diffraction peaks from vanadium species are almost not observed in all samples, indicating that vanadium species are highly dispersed on the surface of ZrP even if vanadium contents on ZrP are loaded as high as 10%.

Fig. 2 shows the morphology of ZrP-derived catalysts revealed by the SEM images. Pristine ZrP reveals its amorphous nanostructure are arranged almost irregular morphology in large domains with rough surface (Fig. 2a). When the vanadium is loaded on ZrP, the amorphous nanostructure seem to become thicker (Fig. 2b), indicating the effect of vanadium introduction. HRTEM is also employed to reveal the morphology of ZrP-derived catalysts (Fig. 3). It is observed that the ZrP support actually consists of some extremely thin nanosheets (50–100 nm), which are stacked together with no special regular structure (Fig. 3a). As presented in Fig. 3b, the P, Zr, V are distributed uniformly on the surface of 2 V/ZrP-m nanosheets as reflected by elemental mapping analysis (Fig. 3e). Moreover, the P, Zr, V on 2 V-ZrP-i catalyst are also observed clearly in spite of slight agglomeration (Fig. 3c and f), as compared with that of 2 V-ZrP-m. Notably, the highly dispersed oligomeric vanadium species are hardly discernable from TEM images (Fig. 3b and c). Moreover, the vanadium species cannot be observed from XRD likely owing to the small size of vanadium species (< 4 nm), which is beyond the detection limit of XRD techniques [37].

Next, the textural properties of catalysts are determined by N_2 adsorption-desorption analysis. The isotherms and pore size distribution curves are displayed in Fig. 4 and corresponding Brunauer-Emmett-Teller (BET) surface area, average pore size and total pore volume results are summarized in Table 1. All of the samples possess a typical type IV isotherm with a clear H1-type hysteresis loop in the relative pressure P/P_0 ranging from 0.8 to 0.9, index of the formation of large amounts of mesoporous structure. The pristine ZrP sample exhibits the highest BET surface area (314 $m^2 g^{-1}$) pore volume (0.57 $cm^3\ g^{-1}$) and pore size (7.2 nm), which reduced obviously due to the addition of vanadium species during the post-treatment (Table 1). Compared to ZrP, the pore diameters of 2 V/ZrP-m and 2 V/ZrP-i decrease to 6.9 and 7.1 nm, respectively. The decrease of pore size can be ascribed to the partial coverage of the larger pores by the highly dispersed vanadium species [38]. On the basis of the analysis above, it suggests that the vanadium modified ZrP by mechanochemical synthesis owns more opening pore than that by the impregnation method, which is in agreement with that of morphology features as seen from the image of HRTEM.

The density and strength of the acid sites (Brönsted and Lewis acid) have a crucial effect on catalytic activity. Therefore, the acidic properties of the catalysts are investigated firstly by NH_3-TPD method, which gain insight into the acidic properties of the catalysts. As displayed in Fig. 5a, in the case of NH_3-TPD profile of ZrP, three desorption peaks are observed in a wide range of temperature from 50 to 700 °C. The peak at temperatures less than 200 °C is attributed to the interaction of the NH_3 with weak acid sites. The shoulder peak observes at temperatures between 200 and 500 °C is attributed to medium strong acid sites, while the high-temperature desorption peak observe at temperatures greater than 500 °C is attributed to strong acid sites [39,40]. The total acidity from the NH_3-TPD patterns for ZrP, 2 V/ZrP-m, 2 V/ZrP-i are found to be 1013.9, 995.3 and 1006.5 μmol g^{-1} respectively (Table 1). The NH_3-TPD patterns of both vanadium-modified ZrP catalysts show two broad desorption peaks. One broad peak centers at 150 °C, and the other around 350 °C represent the weak and medium acid sites, respectively. The latter peak becomes broader and weak dramatically, as compared with the pristine ZrP support, which is suggestive of decreased acidity. Furthermore, the strong acid sites almost disappear after the introduction of vanadium species, suggesting the strong interaction may occur between vanadium precursor and ZrP. Overall, the introduction of vanadium species not only influence the acidic distribution but also decrease the total surface acidity of ZrP.

The nature of acidity is further characterized using pyridine-adsorbed FT-IR spectroscopy which has been recorded in the range of 1800–1400 cm^{-1}. As given in Fig. 5b, pyridine-adsorbed FT-IR spectrum of the ZrP shows a band at 1545 cm^{-1}, which is the characteristic band of the typical pyridinium ion (PyH^+), confirming the presence of Brönsted acid sites, which can be due to the presence of a reasonable amount of P(OH) groups in the ZrP [41]. Further, the band at about 1438 cm^{-1} corresponds to the adsorbed pyridine at the Lewis acid site (PyL), while the band at 1488 cm^{-1} can be attributed to the adsorption of pyridine in both Brönsted and Lewis acid sites [42]. The quantification of acid sites is deduced by using Eqs. (1) and (2), and the results are shown in Table 1. The density of Brönsted acid sites and Lewis acid sites of ZrP are determined as 217.9 μmol g^{-1} and 717.9 μmol g^{-1}, respectively. Particularly, it is found that after the modification by vanadium precursor, the densities of both Lewis acid and the Brönsted acid on the catalysts are reduced. Especially, the density of Brönsted acid sites on the 2 V/ZrP-m catalyst decreases dramatically from 217.9 μmol g^{-1} to 169.2 μmol g^{-1}, accompanying with a decrease of the total acid density (Table 1). In addition, it indicates that as the calcination temperature increasing, both the density of Brönsted (at ~1545 cm^{-1}) and Lewis (~1438 cm^{-1}) acid sites show an obvious decrease on the vanadium-modified ZrP samples (Figure S3). Notably, Brönsted acid sites decrease significantly after calcination at 650 °C, which accounts for the strong interaction between vanadium species and (P—OH) (Brönsted acid sites), most likely due to the formation of V—O—P linkages [37].

The redox properties of the catalysts are crucial for the catalytic oxidation performance. As seen in Fig. 5c, the amorphous ZrP is silent because of no reducible sites. In contrast, 2 V/ZrP-m and 2 V/ZrP-i present only one peak at *ca.* 586 °C and 555 °C respectively, which are attributable to the one-step reduction of the monomeric and/or low oligomeric vanadium species [43]. It is noticeable that the vanadium species on 2 V/ZrP-m are more difficult to be reduced than that on 2 V/

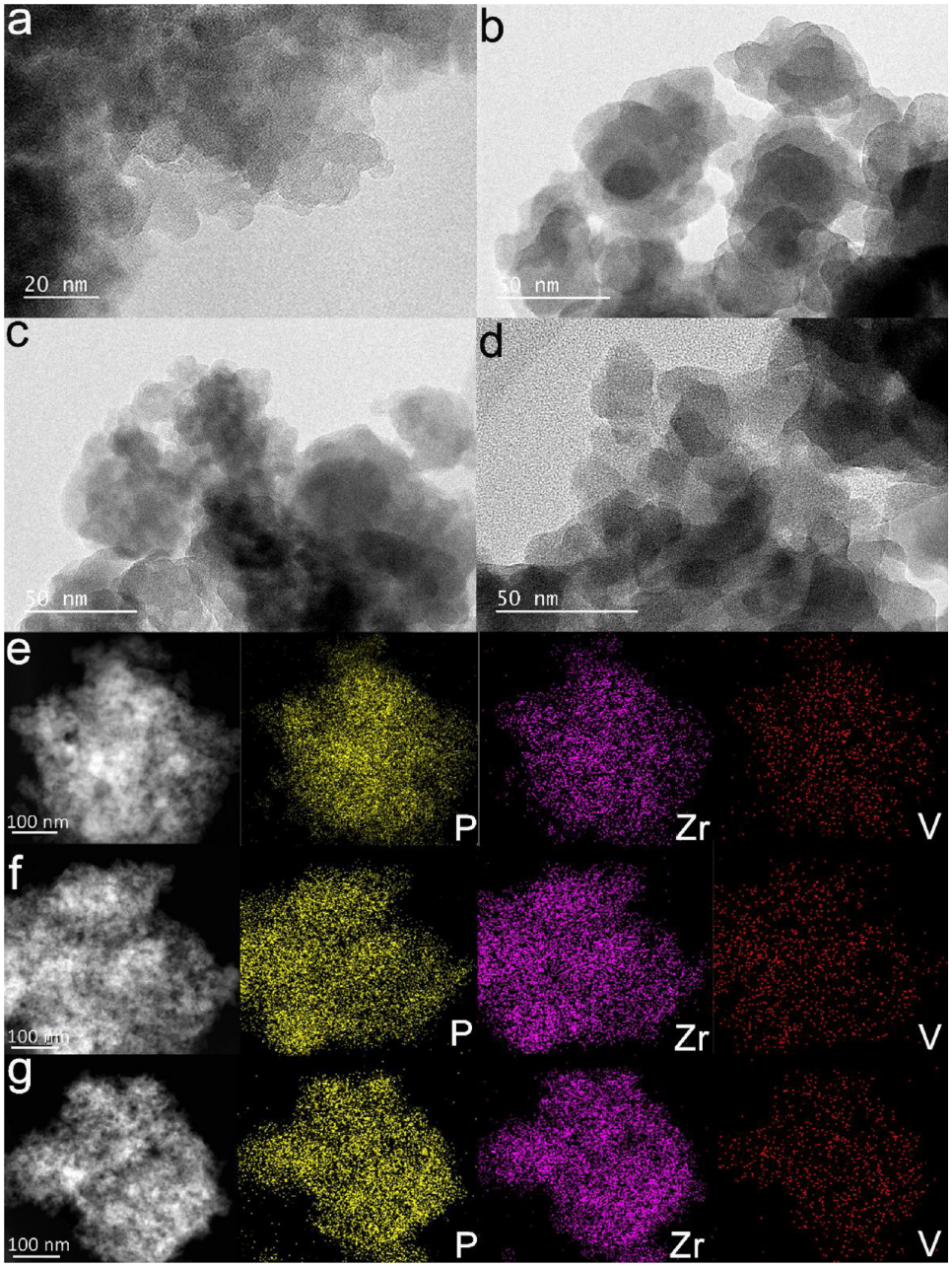

Fig. 3. HRTEM images of (a) ZrP, (b) 2 V/ZrP-m, (c) 2 V/ZrP-i and (d) the spent 2 V/ZrP-m. (e), (f) and (g) are corresponding to the P/Zr/V elemental mappings of 2 V/ZrP-m, 2 V/ZrP-i and the spent 2 V/ZrP-m catalysts, respectively.

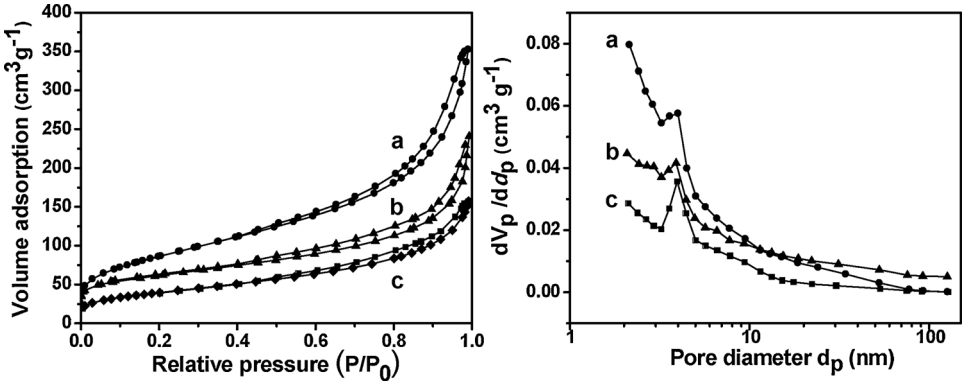

Fig. 4. N_2 adsorption isotherms (left) and pore size distribution curves (right) of (a) ZrP, (b) 2 V/ZrP-m and (c) 2 V/ZrP-i.

Table 1
Physicochemical properties of different catalysts.

Properties	Catalysts		
	ZrP	2 V/ZrP-m	2 V/ZrP-i
S_{BET} ($m^2 g^{-1}$)[a]	314	175	143
V_P (cm^3 g^{-1})[b]	0.57	0.36	0.25
d_{AV} (nm)[c]	7.2	6.9	7.1
Total acidity (μmol NH_3 g^{-1})	1013.9	995.3	1006.5
B acid (μmol g^{-1})[d]	217.9	169.2	181.7
L acid (μmol g^{-1})[e]	717.9	638.1	671.9
L/B	3.29	3.77	3.69
Total acidity (μmol pyridine g^{-1})	935.8	807.3	853.6

[a] BET surface area.
[b] Total pore volume.
[c] Average pore size distribution estimated from BJH method.
[d] B acid = Brönsted acid.
[e] L acid = Lewis acid.

ZrP-i, which reveals that less reducible vanadium species are formed during the reduction process [44]. This may further reflect that the chemical interaction between vanadium species and ZrP support exhibit a great difference on two catalysts.

The surface state of vanadium catalysts is further characterized by XPS. The full survey spectra display similar element species of P, Zr, O and V (Fig. 6a). The XPS spectra of two catalysts present homologous peaks and the observed P 2p and Zr 3d signals centered at 133.8, and 183.3 eV confirm the presence of ZrP structure. In addition, the V $2p_{3/2}$ peaks centered at 517.0–517.3 and 516–516.5 eV, are characteristic of V^{5+} and V^{4+} species [45,46]. As given in Fig. 6b, $2p_{3/2}$ XPS peak for V at 517.3 eV is observed clearly, which indicates that the vanadium is mainly present in the vanadium (V) state with a satellite peak $2p_{1/2}$ at about 254.2 eV. However, a weak peak at 516.4 eV ($2p_{3/2}$) reveals the presence of a tiny amount of the vanadium (IV) species. The existence of this vanadium (IV) phase is possibly due to a residue from the vanadium source ($VOSO_4$) and not completely oxidized to vanadium (V) species. The above results additionally prove that the present 2 V/ZrP-m and 2 V/ZrP-i catalysts enable supported vanadium species exist mainly in its high valence state (V).

Subsequently, the coordination state of the phosphorous center is evaluated by solid ^{31}P MAS NMR spectra. As seen from Fig. 7a, the spectra of the amorphous ZrP shows the three resolved resonance peaks at –11.8 ppm, –19.9 ppm and –26.7 ppm, which can be corresponded to the presence of the tetrahedral phosphates connected with two $[(OH)_2P–(OZr)_2]$ zirconium atom, $[(OH)P–(OZr)_3]$ and phosphate with four P–O–Zr bonds, respectively [47,48]. The three resolved resonance peaks at –11.8 ppm, –19.9 ppm and –28.3 ppm are observed if ZrP was calcined under a higher temperature (550 °C) (Fig. 7b). This indicated the further dehydration process from a partial condensation between –POH and –ZrOH groups could be possible as reflected from a resonance signal shift from –26.9 to –28.3 ppm (Fig. 7a *vs* b).

On one hand, it should be noted that the peak of P–O–Zr linkage shows upfield shifts from –28.3 ppm to –29.6 ppm after vanadium modification (Fig. 7c and d). This can be explained that introduction of vanadium increases the electron density around phosphorus core of ZrP bulk, resulting in the more shielding effect. On the other hand, the peaks at –11.8 ppm and –19.9 ppm become very weak (Fig. 7c and d), reflecting that the introduction of vanadium changes the environment of the phosphate group. Hence, it is highly believable that vanadium modification has a significant effect on the linkage of chemical bond in $(OH)_mP–(OZr)_n$ (m + n = 4). With regard to the results above, a covalent linkage such as $((V—O—P)_m–(OZr)_n)$ has formed (Inset in Fig. 7), which is in accordance with pyridine adsorbed FT-IR spectra that the density of Brönsted acid sites (P—OH) decreased due to vanadium modification, and the presence of the dominant vanadium (V) species from XPS analysis.

3.2. Glycerol oxidation in aqueous phase

The vanadium-modified ZrP catalysts are evaluated for the selective oxidation of glycerol to FA in the aqueous phase under base-free condition. The catalytic activity are obtained in terms of glycerol conversion and product selectivity using molecular oxygen as an oxidant. The

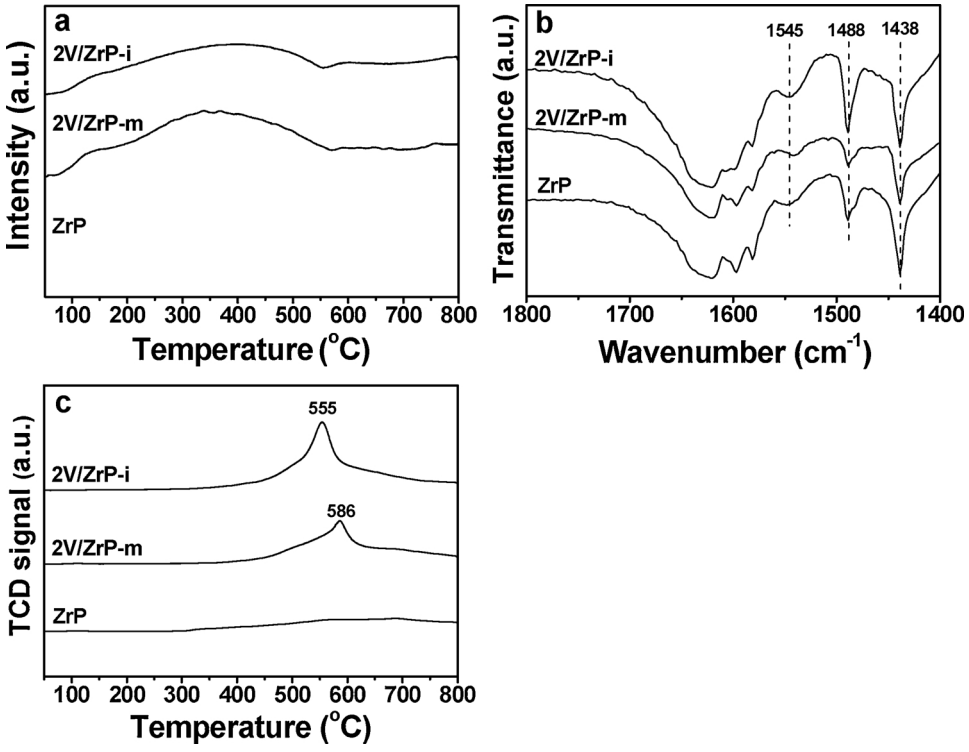

Fig. 5. (a) NH_3-TPD profiles, (b) Pyridine-adsorbed FT-IR spectra and (c) H_2-TPR curves of the different catalysts.

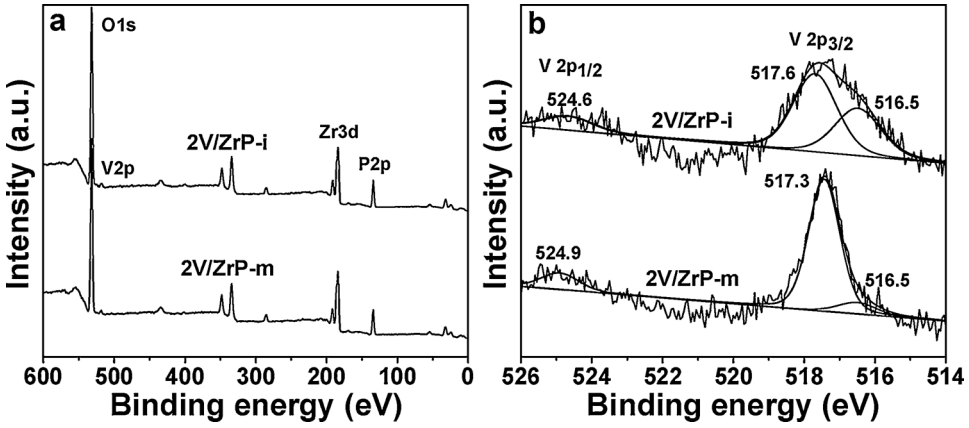

Fig. 6. (a) Survey and (b) V 2p XPS spectra of the vanadium-modified ZrP catalysts.

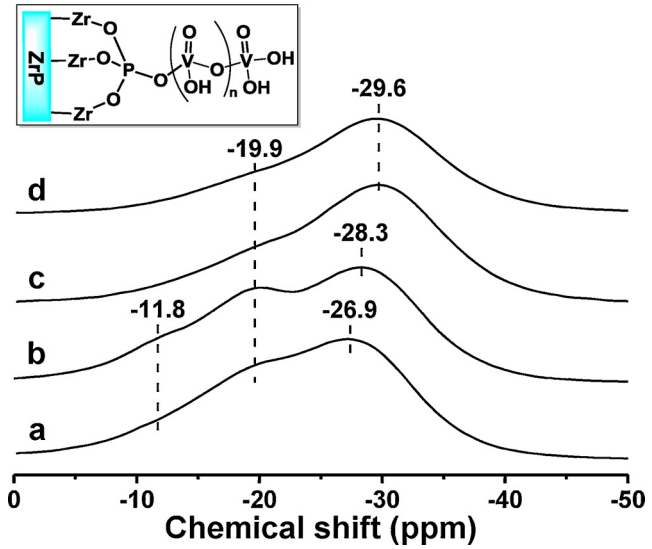

Fig. 7. Solid ^{31}P NMR spectra of (a) ZrP, (b) ZrP was calcined at 550 °C, (c) 2 V/ZrP-m and (d) 2 V/ZrP-i. Inset showed the V–O–P linkage as reflected from ^{31}P NMR spectra and XPS analysis.

Table 2
Catalytic performance of various catalysts for selective oxidation of glycerol.[a]

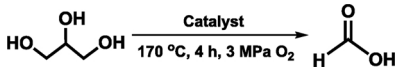

Entry	Catalysts	Con. (%)	Sel. (%)				FA Yield (%)	CMB (%)
			FA	AA	HA	CO_2		
1	None	0	0	0	0	0	0	100
2	$VOSO_4$	89	55	0	1	29.5	49	92.5
3	ZrP	5.1	13.8	11.3	1.6	0	0.7	98.3
4	2 V/ZrP-m	85.6	62.5	6.2	1	18.8	53.5	95.3
5	2 V/ZrP-i	72.4	67.2	4.6	1.5	14.6	48.7	97.6
6[b]	2 V/ZrP-m	0	0	0	0	0	0	100
7	2 V_1/ZrP-m[c]	81.4	57.5	1.1	1.2	23.2	46.8	92.5
8	2 V_2/ZrP-m[d]	81.3	60	5	1.1	21.1	48.8	94.9
9	2 V_3/ZrP-m[e]	80.7	65.6	3.9	1.3	17.3	52.9	95.8

[a] Reaction conditions: 5 mL glycerol aqueous solution (10 wt.%), 25 mg catalyst, 170 °C, 4 h, 3 MPa O_2. FA: formic acid, AA: acetic acid, HA: hydroxyacetone. CMB: Carbon mass balance; [b] 1 MPa N_2; [c–e] NH_4VO_3, $NaVO_3$ and VO $(acac)_2$ have been adopted as vanadium precursors for catalyst preparation, respectively.

catalytic reaction results are listed in Table 2. The reaction does not proceed in the absence of a catalyst or under nitrogen atmosphere, showing an aerobic processes is required for this catalytic system (entries 1 and 6). Control reaction manifests that the vanadium precursor itself ($VOSO_4$) is active for glycerol oxidation and a homogeneous nature is observed visually during the reaction (entry 2). However, in addition to the intrinsic disadvantages of homogeneous catalyst in catalyst recovery and product purification, the homogeneous vanadium compound is unstable and easily hydrolyzes by the water under the present condition [49]. Although the sole ZrP gives low glycerol conversion due to the lack of oxidative sites (entry 3), FA, AA and a trace of HA indeed are detected with 13.8% 11.3% and 1.6% of selectivity, respectively. Notably, the vanadium-modified ZrP catalysts show moderate to good catalytic activity for glycerol oxidation to FA (entries 4, 5, 7–9), which reveals that both acidic sites and oxidizing sites are important for glycerol selective oxidation to FA. Among of them, 2 V/ZrP-m catalyst shows the highest catalytic activity with 85.6% conversion and 62.5% selectivity to FA (entry 4), suggesting that the modification of vanadium species by mechanochemical synthesis provides more efficient approach for glycerol oxidation, as compared with that using incipient wetness method (entries 4 *vs* 5). This could result from the higher molar ratio of L to B on 2 V/ZrP-m catalyst (Table 1), which implies that Lewis acid sites play a more crucial role in activating primary hydroxyl group of glycerol over the present catalysts [50]. Besides, the different vanadium precursors introduced by mechanochemical synthesis seem not to influence the catalytic activity and FA selectivity significantly (entries 7–9), implying that chemical state of vanadium on ZrP support can be similar after calcination in spite of the different vanadium sources. It was found that a certain amount of CO_2 derived from the overoxidation was detected (Table 2). Notably, the vanadium-modified ZrP catalysts seemed to suppress effectively the formation of CO_2, as compared with that of a sole $VOSO_4$ (entries 2, 4 and 5). Besides, as shown in Table 2, although carbon mass balance of the glycerol oxidation was normally higher than 92%, the formation of a small amount of polymer or coking under the present reaction condition could not be excluded [51,52]. After reaction, the spent 2 V/ZrP-m catalyst was subjected to TGA analysis (Figure S5). It can be seen that the spent 2 V/ZrP-m showed a weight loss (10.8%), which actually was close to that of the fresh one (9.2%). This revealed that the coking might be not a very serious problem on the present catalyst.

The reaction conditions are optimized by systematically exploring the influence of various reaction parameters, including reaction temperature, time, pressure, vanadium loadings on ZrP support and the reaction results are shown in Fig. 8. The reaction is normally performed over 2 V/ZrP-m catalysts due to its high catalyst performance as demonstrated Table 2. It can be seen that as the reaction temperature varies from 140 to 180 °C, the conversion of glycerol and the FA selectivity increases significantly, accompanying with the formation of a

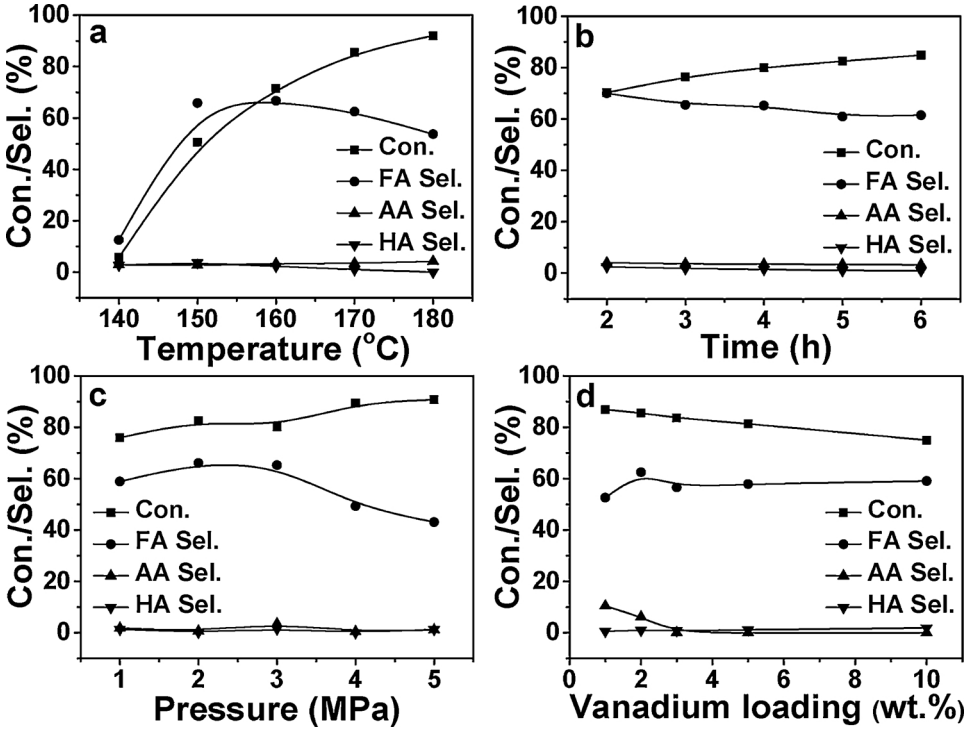

Fig. 8. Influence of (a) reaction temperature, (b) reaction time, (c) pressure and (d) vanadium loading on catalytic activity for selective oxidation of glycerol over 2 V/ZrP-m catalyst. Reaction conditions: 5 mL glycerol aqueous solution (10 wt.%), 25 mg catalyst, 170 °C, 4 h, 3 MPa O_2.

trace of AA and HA (Fig. 8a). However, the FA selectivity affords an optimum around 150 °C, and then decreases slightly with higher temperature, revealing that FA cannot be stable and decompose into CO_2 at high reaction temperature. The current oxidation reaction actually happens quite quickly at 170 °C, giving 70% conversion and 70% selectivity of HA within 2 h (Fig. 8b), but the FA selectivity declines slightly with the prolonged time up to 4 h because of the decomposition of FA. The oxygen pressure has a positive effect on conversion of glycerol when oxygen pressure is below 3 MPa. Nevertheless, higher oxygen pressure brings about lower yield of FA due to the occurrence of over-oxidation reaction (Fig. 8c). GC analysis confirms that CO_2 is indeed present in gas phase, but no CO is detected. Furthermore, it is found that the vanadium loadings on ZrP support have a negative impact on the conversion of glycerol but a complicated influence on the selectivity of FA (Fig. 8d). Especially, when the vanadium loadings is over 2%, the negative effect on FA selectivity is observed, which reveals that the presence of excess of the vanadium species on ZrP surface contributes to decomposition of FA. Overall, the reaction can be proceeded smoothly over 2 V/ZrP-m under 170 °C, 4 h and 3 MPa O_2 conditions.

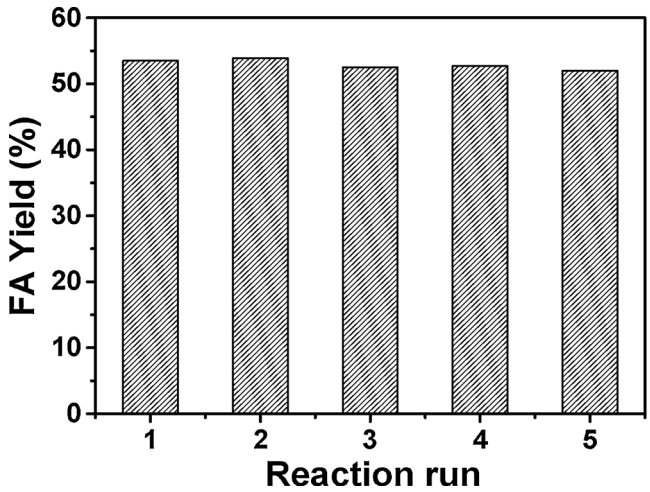

Fig. 9. Catalytic recyclability over 2 V/ZrP-m for selective oxidation of glycerol. Reaction conditions: 5 mL glycerol aqueous solution (10 wt.%), 25 mg catalyst, 170 °C, 4 h, 3 MPa O_2.

3.3. Catalyst recycling

The reusability of the catalysts is determined because catalyst recyclability exhibits an indispensable part in the catalytic performance evaluation of compound transformations. The 2 V/ZrP-m catalyst has been employed for evaluating catalytic reusability in glycerol oxidation. In each cycle, the catalyst can be facilely recovered by centrifugation from the reaction mixture, followed by washing with deionized water and dry at 100 °C for 12 h, and then sintering at 550 °C for 3 h. The recovered catalyst can be reused directly in the subsequent run without adding fresh catalyst. In a five-run recycling test, no apparent decline of FA yield is observed, confirming the excellent reusability of the catalyst (Fig. 9). The XRD pattern of the spent catalyst after the 5th run (Fig. 1e) is almost the same as that of the fresh one. The image of SEM displays no obvious difference between the fresh and spent catalyst (Fig. 2b *vs* c), although a slight aggregation of vanadium species occur from HRTEM image and the elemental mapping (Fig. 3e and g). ICP-AES analysis results indicate the leaching of the vanadium species is neglectable (< 50 ppm), which reveals that the current 2 V/ZrP-m catalyst is highly stable and leaching-resistant even under aqueous phase condition. The excellent recyclability of the present vanadium-modification catalyst clearly arises from the robust immobilization of vanadium by forming V–O–P linkages on ZrP surface, as reflected by the determination of Brönsted acid sites (Table 1) and solid ^{31}P NMR spectra (Fig. 7). Overall, the ZrP support not only retains the oxidation activity of vanadium species but also enhances the stability due to the strong covalent interaction.

3.4. Insight into the reaction mechanism

The reactivity of different substrates over 2 V/ZrP-m catalyst has been investigated in order to understand the possible pathway, the representative substrate molecules including EG, HA, DHA and AA are employed for oxidation under the same reaction conditions. The reaction results are summarized in Table S1. It is found that EG affords a low reactivity, but offers 46.6% selectivity toward to FA (entry 1). Both HA and DHA are proved to be highly reactive molecules for oxidation, leading to the formation of FA and AA (entries 2 and 3). However, AA cannot be oxidized under the present condition (entry 4). This result indicates that both of FA and AA are ultimate oxidation product and HA may be the intermediate of glycerol oxidation. Notably, the present catalyst can be applicable to the oxidation of high glycerol concentration in aqueous solution (20 wt.%), which provides 89% glycerol conversion and 63.6% selectivity to FA (entry 5).

As indicated above, the vanadium-modified catalyst 2 V/ZrP-m exhibits superior catalytic performance in the selective oxidation of glycerol in the aqueous phase under base-free condition, affording the conversion and FA selectivity as high as 85.6% and 62.5%, respectively. The highly active, stable oxidative sites on the 2 V/ZrP-m catalyst is firstly attributed to large surface area, which enables the good dispersion of active oxidative sites and good accessibility to the substrates, accelerating mass transfer in the catalytic process. Besides, the covalent interaction between vanadium species and the surface P(OH) groups on ZrP contributes to the excellent catalytic stability.

It should be pointed out that the vanadium species on the ZrP surface are the catalytically active sites for glycerol oxidation. The active sites are highly related with the chemical state of vanadium on the ZrP surface. Thus one problem arises whether the concentration of vanadium (V) on the surface is a decisive factor on catalytic activity. With regard to this issue, the 2 V/ZrP-m catalyst has subjected to different calcination temperature and the XPS spectra of the corresponding catalysts are presented in Figure S4. Interestingly, the contents of vanadium (V) species increase with the calcination temperature, indicating that the calcination at higher temperature is favorable to forming more vanadium (V) species. However, the high temperature calcination can also results in the aggregation of the active vanadium species, the calcination temperature is set to less than 650 °C in this work. The concentration of vanadium (V) species on surface is derived from the XPS spectra (Fig. 6 and Figure S4) and summarized in Table 3. It demonstrates clearly that FA yield is highly relevant to the concentration vanadium (V) species, the higher vanadium (V) species, the higher FA yield.

To identify the intermediate product of this reaction, solid ^{13}C NMR spectra is carried out on the glycerol-absorbed. As shown in Fig. 10a, the resonance signal at 66.6 and 76.2 ppm can be attributed to the primary carbon and secondary carbon atom of glycerol molecule [53], respectively. New signals are appeared after the glycerol-absorbed is further subjected to heating under the air. As depicted in Fig. 10b, a clear signal at 23.5 ppm is observed, matching with methyl group of hydroxyacetone or pyruvic acid. The resonance peaks ranging from 165 to 195 ppm result from carbonyl groups of aldehydes, carboxylic acids and ketones, while the characteristic peak at 95.2 ppm is assigned to the

Table 3
The effect of surface vanadium (V) concentration on vanadium-modified ZrP catalysts for FA yield.

Catalysts	$V^{5+}/(V^{5+}+V^{4+})$[a]	Con. (%)	FA Yield (%)
2 V/ZrP-m, calcined at 350 °C	0.56	58.3	35.3
2 V/ZrP-m, calcined at 450 °C	0.61	66.9	42.2
2 V/ZrP-i, calcined at 550 °C	0.70	72.4	48.7
2 V/ZrP-m, calcined at 550 °C	0.90	85.6	53.5
2 V/ZrP-m, calcined at 650 °C	0.99	87.7	57.6

[a] The values were determined by XPS analysis.

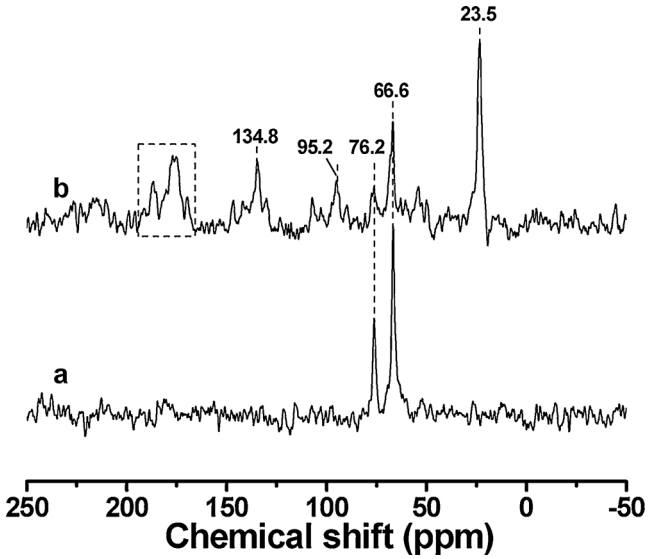

Fig. 10. Solid ^{13}C NMR spectra of the glycerol-absorbed on 2 V/ZrP-m catalyst. (a) Glycerol (15 wt.%) was absorbed on catalyst by immersing catalyst in glycerol solution of methanol, followed by drying for 1 h under the vacuum at 30 °C; (b) After (a) procedure, the sample was heated at 70 °C under the air.

secondary carbon atom of glyceraldehyde. Moreover, a signal at 134.8 ppm corresponds with C—C double bond in acrolein molecule [54,55], which is well consistent with the previous results originated from dehydration of glycerol to 3-hydroxypropanal, followed by the further dehydration to acrolein [56,57].

Based on the activity evaluation and solid ^{13}C NMR characterization, a possible reaction pathway on the present catalysts is proposed, as shown in Scheme 1. There are two possible reaction pathways to generate FA. The first route involves in Lewis acid-catalyzed dehydration of glycerol into hydroxyacetone, which is further oxidized to pyruvic acid and then degrades into FA and AA by C—C cleavage, respectively [58]. In the second route, glycerol first was dehydrogenated into glyceraldehyde or dihydroxyacetone on active vanadium (V) species, and these compounds are instable intermediate which can then be oxidized to glyceric acid, and then underwent carbon-carbon cleavage and further oxidation to oxalic acid. Since the two carboxyl groups in oxalic acid are in adjacent positions and not very stable, decarboxylation is possible and formed further to FA [59–61]. However, FA could be decomposed into CO_2 under the present reaction condition (Scheme 1). Thus, to examine the stability of FA in this catalytic system, FA (10 wt.% in water) is used as the substrate under the same oxidation conditions, and it is found that only 13.8% of FA is decomposed. This result reveals that FA is rather stable in this catalytic system, leading to high selectivity towards FA (Table 2) [32].

Overall, this is the first time that vanadium-modified ZrP by mechanochemical synthesis has demonstrated a considerable activity for selective oxidation of glycerol. The superior performance can be attributed to the high dispersion of vanadium species on the ZrP surface; such active sites are easily accessible to the substrate, thus dramatically promoting the oxidation of glycerol into FA.

4. Conclusions

Vanadium modified-ZrPs are directly synthesized from an environmentally friendly mechanochemical synthesis strategy and serve as highly efficient catalyst. The as-obtained 2 V/ZrP-m catalyst exhibits high glycerol conversion (85.6%) and FA yield (53.5%), as well as good reusability for the liquid phase oxidation of glycerol. The remarkable performance results from the strong covalent interaction of ZrP with vanadium species that enable active vanadium species to be highly

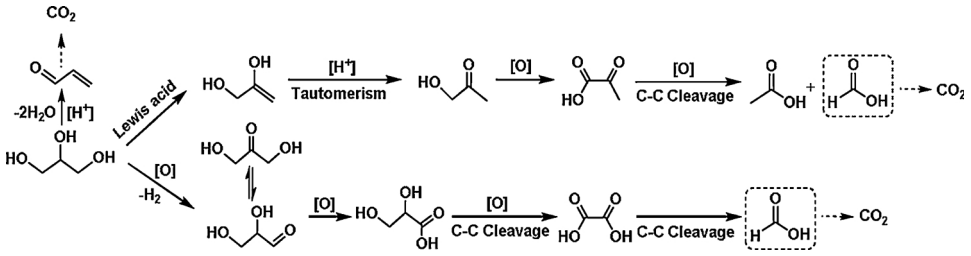

Scheme 1. Reaction mechanism for selective oxidation of glycerol to FA.

dispersed on surface, promoting both the activity and the stability of catalyst. It demonstrates that Lewis acid sites of ZrP support exert a great effect on glycerol activation, and meanwhile vanadium species are responsible for glycerol dehydrogenation and subsequent oxidation of the instable intermediates. The catalysts prepared with different methods allow us to shed light on the relationship between the properties and catalytic activity. Notably, solvent-free and cost-effective route for catalyst preparation are of paramount importance from the practical point of view. This work provides a new alternative synthetic route to fabricate non-noble metal doped ZrP heterogeneous catalyst for biomass conversion to important commodity chemicals.

Acknowledgements

The authors are grateful for support from the National Natural Science Foundation of China (21373082, 21773061) and Innovation Program of Shanghai Municipal Education Commission (15ZZ031), and the Fundamental Research Funds for the Central Universities.

Appendix A. Supplementary data

Supplementary material related to this article can be found, in the online version, at doi:https://doi.org/10.1016/j.mcat.2019.110404.

References

[1] A. Corma, S. Iborra, A. Velty, Chem. Rev. 107 (2007) 2411–2502.
[2] A. Villa, N. Dimitratos, C.E. Chan-Thaw, C. Hammond, L. Prati, G.J. Hutchings, Acc. Chem. Res. 48 (2015) 1403–1412.
[3] Y.H. Tan, M.O. Abdullah, C. Nolasco-Hipolito, Renew. Sust. Energ. Rev. 47 (2015) 589–603.
[4] J.J. Bozell, G.R. Petersen, Green Chem. 12 (2010) 539–554.
[5] J.M. Clomburg, R. Gonzalez, Trends Biotechnol. 31 (2013) 20–28.
[6] C.H. Zhou, H. Zhao, D.S. Tong, L.M. Wu, W.H. Yu, Catal. Rev. Sci. Eng. 55 (2013) 369–453.
[7] M. Anitha, S.K. Kamarudin, N.T. Kofli, Chem. Eng. J. 295 (2016) 119–130.
[8] P.S. Kong, M.K. Aroua, W.M.A. Wan Daud, Rev. Chem. Eng. 31 (2015) 437–552.
[9] B.S. Sánchez, M.S. Gross, C.A. Querini, Catal. Today 296 (2017) 35–42.
[10] J. Fu, Q. He, P.J. Miedziak, G.L. Brett, X. Huang, S. Pattisson, M. Douthwaite, G.J. Hutchings, Chem. Eur. J. 24 (2018) 2396–2402.
[11] X. Ning, Y. Li, H. Yu, F. Peng, H. Wang, Y. Yang, J. Catal. 335 (2016) 95–104.
[12] G.L. Brett, Q. He, C. Hammond, P.J. Miedziak, N. Dimitratos, M. Sankar, A.A. Herzing, M. Conte, J.A. Lopez-Sanchez, C.J. Kiely, D.W. Knight, S.H. Taylor, G.J. Hutchings, Angew. Chem. Int. Ed. 50 (2011) 10136–10139.
[13] E. Skrzyńska, S. Zaid, A. Addad, J.-S. Girardon, M. Capron, F. Dumeignil, Catal. Sci. Technol. 6 (2016) 3182–3196.
[14] G. Dodekatos, H. Tüysüz, ChemCatChem 9 (2017) 610–619.
[15] X. Jin, M. Zhao, C. Zeng, W. Yan, Z. Song, P.S. Thapa, B. Subramaniam, R.V. Chaudhari, ACS Catal. 6 (2016) 4576–4583.
[16] E. Farnetti, C. Crotti, Catal. Commun. 84 (2016) 1–4.
[17] R. Palacio, S. Torres, D. Lopez, D. Hernandez, Catal. Today 302 (2018) 196–202.
[18] S. Schünemann, F. Schüth, H. Tüysüz, Catal. Sci. Technol. 7 (2017) 5614–5624.
[19] M. Grasemann, G. Laurenczy, Energy Environ. Sci. 5 (2012) 8171–8181.
[20] H.W. Gibson, Chem. Rev. 69 (1969) 673–692.
[21] P. Preuster, J. Albert, Energy Technol. 6 (2018) 501–509.
[22] T. Lu, M. Niu, Y. Hou, W. Wu, S. Ren, F. Yang, Green Chem. 18 (2016) 4725–4732.
[23] X. Liu, S. Li, Y. Liu, Y. Cao, Chin. J. Catal. 36 (2015) 1461–1475.
[24] R.R. Langeslay, D.M. Kaphan, C.L. Marshall, P.C. Stair, A.P. Sattelberger, M. Delferro, Chem. Rev. 119 (2019) 2128–2191.
[25] R. Wölfel, N. Taccardi, A. Bösmann, P. Wasserscheid, Green Chem. 13 (2011) 2759–2763.
[26] J. Li, D.-J. Ding, L. Deng, Q.-X. Guo, Y. Fu, ChemSusChem 5 (2012) 1313–1318.
[27] J. Zhang, M. Sun, X. Liu, Y. Han, Catal. Today 233 (2014) 77–82.
[28] J. Reichert, B. Brunner, A. Jess, P. Wasserscheid, J. Albert, Energy Environ. Sci. 8 (2015) 2985–2990.
[29] M. Niu, Y. Hou, W. Wu, S. Ren, R. Yang, Phys. Chem. Chem. Phys. 20 (2018) 17942–17951.
[30] M. Niu, Y. Hou, S. Ren, W. Wu, K.N. Marsh, Green Chem. 17 (2015) 453–459.
[31] M. Yuan, D. Li, X. Zhao, W. Ma, K. Kong, W. Ni, Q. Gu, Z. Hou, Acta Phys. Chim. Sin. 34 (2018) 886–895.
[32] J. Zhang, M. Sun, Y. Han, RSC Adv. 4 (2014) 35463–35466.
[33] D. Li, W. Ni, Z. Hou, Chin. J. Catal. 38 (2017) 1784–1793.
[34] H. Xiao, S. Liu, Mater. Design 155 (2018) 19–35.
[35] Y. Kamiya, S. Sakata, Y. Yoshinaga, R. Ohnishi, T. Okuhara, Catal. Lett. 94 (2004) 45–47.
[36] M. Assefi, M. Torabi, A. Sajadi, J. Chin. Chem. Soc. 64 (2017) 164–175.
[37] N.P. Rajan, G.S. Rao, V. Pavankumar, K.V.R. Chary, Catal. Sci. Technol. 4 (2014) 81–92.
[38] H. Chen, Y. Xia, H. Huang, Y. Gan, X. Tao, C. Liang, J. Luo, R. Fang, J. Zhang, W. Zhang, X. Liu, Chem. Eng. J. 330 (2017) 1195–1202.
[39] A.M. Camiloti, S.L. Jahn, N.D. Velasco, L.F. Moura, D. Cardoso, Appl. Catal. A Gen. 182 (1999) 107–113.
[40] D. Verma, B.S. Rana, R. Kumar, M.G. Sibi, A.K. Sinha, Appl. Catal. A Gen. 490 (2015) 108–116.
[41] W. Ni, D. Li, X. Zhao, W. Ma, K. Kong, Q. Gu, M. Chen, Z. Hou, Catal. Today 319 (2019) 66–75.
[42] P. Sreenivasulu, N. Viswanadham, T. Sharma, B. Sreedhar, Chem. Commun. 50 (2014) 6232–6235.
[43] C.K.P. Neeli, V.S.P. Ganjala, V. Vakati, K.S.R. Rao, D.R. Burri, New J. Chem. 40 (2016) 679–686.
[44] A. Held, J. Kowalska-Kuś, K. Nowińska, K. Góra-Marek, J. Catal. 347 (2017) 21–35.
[45] B.P. Barbero, L.E. Cadús, L. Hilaire, Appl. Catal. A Gen. 246 (2003) 237–242.
[46] T. Gao, Z. Jin, M. Liao, J. Xiao, H. Yuan, D. Xiao, J. Mater. Chem. A Mater. Energy Sustain. 3 (2015) 17763–17770.
[47] Y. Zhu, T. Shimizu, T. Kitajima, K. Morisato, N. Moitra, N. Brun, T. Kiyomura, K. Kanamori, K. Takeda, H. Kurata, M. Tafu, K. Nakanishi, New J. Chem. 39 (2015) 2444–2450.
[48] A. Sinhamahapatra, N. Sutradhar, B. Roy, A. Tarafdar, H.C. Bajaj, A.B. Panda, Appl. Catal. A Gen. 385 (2010) 22–30.
[49] J. . Krakowiak, D. Lundberg, I. Persson, Inorg. Chem. 51 (2012) 9598–9609.
[50] M. Velasquez, A. Santamaria, C. Batiot-Dupeyrat, Appl. Catal. B Environ. 160 − 161 (2014) 606–613.
[51] C.S. Carriço, F.T. Cruz, M.B. dos Santos, D.S. Oliveira, H.O. Pastore, H.M.C. Andrade, A.J.S. Mascarenhas, J. Catal. 334 (2016) 34–41.
[52] S. Veiga, J. Bussi, Energ. Convers. Manage. 141 (2017) 79–84.
[53] N.H.T. Nguyen, A. Brathe, B. Hassel, J. Neurochem. 85 (2003) 831–842.
[54] F. García-Jiménez, O.C. Zúñiga, Y.C. García, J. Cárdenas, G. Cuevas, J. Braz. Chem. Soc. 16 (2005) 467–476.
[55] C. Delseth, T.T.-T. NguyIn, J.-P. Kintzin, Helv. Chim. Acta 63 (1980) 498–503.
[56] H. Gan, X. Zhao, B. Song, L. Guo, R. Zhang, C. Chen, J. Chen, W. Zhu, Z. Hou, Chin. J. Catal. 35 (2014) 1148–1156.
[57] B. Katryniok, S. Paul, F. Dumeignil, ACS Catal. 3 (2013) 1819–1834.
[58] S. Célerier, S. Morisset, I. Batonneau-Gener, T. Belin, K. Younes, C. Batiot-Dupeyrat, Appl. Catal. A Gen. 557 (2018) 135–144.
[59] R. Nie, D. Liang, L. Shen, J. Gao, P. Chen, Z. Hou, Appl. Catal. B Environ. 127 (2012) 212–220.
[60] D. Liang, J. Gao, H. Sun, P. Chen, Z. Hou, X. Zheng, Appl. Catal. B Environ. 106 (2011) 423–432.
[61] Y. Sun, X. Li, J. Wang, W. Ning, J. Fu, X. Lu, Z. Hou, Appl. Catal. B Environ. 218 (2017) 538–544.